

Nucleation and Growth in the Collapsed Langmuir Monolayers from Semifluorinated Alkanes

Marcin Broniatowski,^{*,†} Nuria Vila-Romeu,[‡] Marina Nieto-Suarez,[‡] and Patrycja Dynarowicz-Łątka[†]

Faculty of Chemistry, Jagiellonian University, Ingardena 3, 30-060 Kraków, Poland, and Faculty of Sciences, Department of Physical Chemistry, University of Vigo, Campus Ourense, As Lagoas s/n, 32004 Ourense, Spain

Received: June 21, 2007; In Final Form: September 2, 2007

The 3D phase formation was monitored in relaxation experiments of the collapsed Langmuir monolayers of selected partially fluorinated tetracosanes, that is, F6H18, F8H16, and F10H14. To carry out these experiments, the classical method of surface manometry, such as π -A isotherms registration and the molecular area–time dependencies, under quasi-static monitoring conditions were applied. The evolution of 3D structures at the water/air interface was observed with Brewster angle microscopy (BAM). The obtained data were interpreted according to the nucleation–growth–collision theory model. It occurred that, even though the investigated chemicals are not classical surfactants and do not possess any polar headgroup, their evolution from a 2D monolayer to 3D structures can be successfully modeled with the above-mentioned theory. The influence of the subphase temperature on the nucleation process is also discussed.

Introduction

When a water-insoluble surfactant is spread from its solution in a volatile organic solvent onto the air/water interface, the Langmuir monolayer is created.¹ Such a film is often considered to have a two-dimensional (2D) structure; however, the reduction of the dimensionality does not lead whatsoever to any simplicity of its physicochemical behavior. In contrast, a plethora of physical phenomena can be observed in Langmuir monolayers. Analogously—as in the bulk—phase transitions can also be observed in Langmuir monolayers: the film-forming molecules can be organized as a 2D gas, 2D liquid, or 2D solid. The possibility of 2D mesophase occurrence makes the phase diagrams for monolayers even more complicated.^{2,3} When a monolayer is being further compressed in its solid state, at a particular value of molecular area, there is not enough room at the surface to accommodate all the film molecules in a 2D arrangements. As a result, film molecules separate from the monolayer and form a 3D phase. This transformation is referred to as a monolayer collapse. Macroscopically, it is experimentally registered as an abrupt change of the course of the surface pressure–area curve, seen either as a sharp surface pressure drop (spike) or a plateau formed in the course of the compression isotherm after reaching the maximum surface pressure value.⁴ Although the collapse pressure (π_c) corresponds to the highest surface pressure value observed upon film compression, it should be pointed out that the formation of the 3D phase normally begins not exactly at π_c , but below its value. Therefore, the whole compression isotherm of a monolayer can be divided into two regions: the first one, at which the monolayer is stable, and the second one, at which the monolayer is metastable. This is related to the idea of equilibrium surface pressure (ESP), defined as a π -value, at which the monolayer and the 3D phase are in thermodynamic equilibrium. In his monography, Gaines¹

has defined another parameter important for the Langmuir monolayer characterization—the critical surface pressure (π_{crit}). This is the pressure at which, under particular experimental conditions, the first 3D structures start to separate from the monolayer. If the monolayer compression rate was infinitely slow, these three different pressure values would coincide, but for a real experimental condition, $ESP < \pi_{crit} < \pi_c$. Therefore, the collapse pressure can be defined as the point in the compression isotherm at which the rate of compression equals the rate of 3D phase formation.

The collapse of monolayers and its mechanism was a subject of a plethora of scientific publications, as it is crucial for monolayer description as well as important in thin-film technology. The most frequently studied model systems are the lung surfactant^{5–8} and the monolayers of long-chain carboxylic acids.^{4,9–12} The collapse and its reversibility is especially important in the former case, as the production of the artificial lung surfactant used for the treatment of prematurely born children, whose lungs do not develop the natural one, is an important task for pharmacists and leads to extensive investigations of this system, where special emphasis is put on monolayer relaxation and the collapse mechanism. On the other hand, the investigation of the monolayers of carboxylic acids^{4,9–12} were of great importance in understanding the collapse phenomenon. Namely, it came out that the means of monolayer collapse is a resultant of the molecular properties, subphase composition, and experimental conditions. On the basis of the experimental works, different models of the monolayer collapse have been elaborated. Chronologically, the first model was proposed by Ries.¹³ The collapse was described as a process during which, after a sequence of weakening, folding and bending of the folded monolayer, a trilayer (a bilayer formed on the top of a monolayer) is formed. In the early eighties of the preceding century, Smith and Berg¹⁴ proposed a different model of film collapse, ascribing this phenomenon to the 3D nucleation of the 2D film. Most-elaborated and best-verified experimentally is, however, the nucleation–growth–collision theory presented

* Corresponding author. Tel. +48-12-6632082. Fax: +48-12-6340515. E-mail: broniato@chemia.uj.edu.pl.

[†] Jagiellonian University.

[‡] University of Vigo.

by Vollhardt and his co-workers.^{15–17} In this theory, the overall rate of nucleation and growth of the 3D phase is the convolution of the nucleation and growth rates. As limiting cases of the model, different starting geometries of the growing nuclei are considered. In the latest improved version of the theory, the so-called lenticular growth of the nuclei was discussed and the limitations regarding the geometry of the growing centers were eliminated.^{18–19} The nucleation–growth–collision theory provided a powerful mathematical tool for the discussion of the monolayer collapse phenomenon, and it was applied by a number of authors^{4,20} for the analysis of their experimental results.

In this paper, we focus our attention on the collapse and relaxation phenomena of monolayers formed by nontypical surfactants, that is, films from semifluorinated alkanes. Semifluorinated alkanes (SFAs) are simple diblock molecules comprised of a hydrocarbon chain covalently bound to a perfluorinated segment. The $-\text{CH}_2-\text{CF}_2-$ bond creates a significant dipole moment in such a molecule, which, together with quite different structures of both of its constituting moieties, leads to the situation that SFAs behave as primitive surfactants, although they do not possess any polar headgroup. SFAs are known to self-organize in solutions,²¹ form Gibbs monolayers at the oil/air interface²² as well as Langmuir monolayers at the water/air interface,²³ and to self-assemble into very interesting structures when deposited onto solid substrates.²⁴ Although pure^{25,26} and mixed^{27,28} Langmuir monolayers of SFAs have already been investigated, to-date the collapse mechanism of such monolayers and its evolution at constant surface pressures have not been studied. Therefore, the aim of this paper is to fulfill this gap. For our research, three compounds have been selected; these compounds are fluorinated derivatives of the normal alkane—tetracosane. Since they were already investigated by us in pure²⁹ and mixed monolayers,³⁰ this contribution is a natural continuation of the former works. Namely, we compare here the 2D-to-3D transition for 1,1,1,2,2,3,3,4,4,5,5,6,6-tridecafluorotetracosane (F6H18); 1,1,1,2,2,3,3,4,4,5,5,6,6,7,7,8,8-heptafluorotetracosane (F8H16); and 1,1,1,2,2,3,3,4,4,5,5,6,6,7,7,8,8,9,9,10,10-heneicosfluorotetracosane (F10H14). To reach our goal, we applied the surface pressure (π)–mean molecular area (A) isotherms and the relaxation experiments of the monolayers close to the collapse pressure (the molecular area evolution in time at a constant surface pressure). Upon the whole relaxation time, the evolution of the investigated monolayers was observed with Brewster angle microscopy (BAM) in polarized light. The observations were followed by the application of the nucleation–growth–collision theory to have a deeper insight into the relaxation phenomena and to verify the applicability of this theory to nontypical surfactants.

Experimental Section

In the present research we used the same samples of SFAs as described in previous investigations,^{29,30} synthesized by one of us (M.B.), according to the procedure of Rabolt et al.³¹ The synthesis and purification of these chemicals are described elsewhere.³² The investigated chemicals are white, waxy solids at room temperature, and their melting temperatures are the following: 40 °C (F6H18), 52 °C (F8H16), and 67 °C (F10H14). No thermotropic liquid-crystalline behavior was found for these SFAs, in contrast to the homologues with shorter hydrocarbon moieties.^{29,32} The investigated semifluorinated alkanes were dissolved in chloroform (Spectroscopic grade, Aldrich) in concentration of about 0.5 mg/mL. The solutions were spread on the ultrapure water surface (Milli-Q, resistivity

> 18.2 M Ω) with a 100 μL Hamilton microsyringe. All the experiments were carried out on the 601-BAM Langmuir trough (NIMA, Coventry, UK) of a total area of 500 cm^2 equipped with two Teflon barriers enabling symmetrical compression. The surface pressure was monitored continuously by the Wilhelmy electronic microbalance with the accuracy of ± 0.1 mN/m using a paper plate made of Whatman ashless chromatographic paper as the pressure sensor. The Langmuir trough was thermostated with a Julabo circulating water bath with an accuracy of ± 0.1 °C. In each experiment, 10 min were left after the spreading of the SFA solution for chloroform evaporation, after which the compression of the monolayer with a rate of 30 cm^2/min was initiated. This particular value of compression velocity was chosen after a series of experiments in which the influence of compression rate on the isotherm characteristics, with special emphasis on the collapse behavior, was studied. It occurred that when the compression speed was higher than 50 cm^2/min , it profoundly affected the collapse characteristics; however, within the range of 10–50 cm^2/min , the influence of the compression rate on the collapse characteristics was negligible and we decided to apply the compression speed of 30 cm^2/min in all routine experiments. In relaxation experiments, the monolayers were compressed to a particular surface pressure value (specified in the text), at which the compression was slowed down to the quasi-static conditions, at which the achieved surface pressure was invariant and the evolution of the molecular area in time was observed. All π – A isotherms as well as all A – $\log t$ relaxation curves presented in this study are averages of at least three independent experiments.

A Brewster angle microscope BAM 2 plus (NFT, Germany) was used for microscopic observation of the monolayer structure. It is equipped with a 50 mW laser, emitting p -polarized light of 532 nm wavelength, which is reflected off the air–water interface at approximately 53.15° (Brewster angle). The lateral resolution of the microscope was 2 μm . The images were digitized and processed to obtain the best quality of the BAM pictures. Each image corresponds to a 770 $\mu\text{m} \times 570 \mu\text{m}$ monolayer fragment. All the applied equipment was placed on an antivibration table.

Results

The relaxation measurements have been carried out at 10, 20, and 30 °C to monitor how the change in subphase temperature affects the collapse and its evolution in time. The π – A isotherms recorded at different temperature values for the three investigated compounds are presented in Figure 1. For F10H14 and F8H16, the surface pressure starts to rise at ca. 0.4 $\text{nm}^2/\text{molecule}$ and monolayers collapse at about 0.32 $\text{nm}^2/\text{molecule}$, whereas for F6H18 these values are shifted slightly toward the lower molecular areas. The influence of the subphase temperature on the SFA monolayer organization is clearly visible, manifesting itself in the decrease of the collapse pressure value and some shifts of the isotherm toward lower molecular areas upon the temperature rise. The state of the monolayers at the investigated three temperatures can be inferred from the C_s^{-1} – π plots (see Figure 1 insets) (compression modulus of a monolayer is defined as follows $C_s^{-1} = -A \, d\pi/dA$), which—during the compression of the films—do not exceed the value of 100 mN/m (the lower limit of the liquid-condensed phase existence³³). Two general types of collapse are known: the spike-like collapse and the plateau-like collapse.⁴ In the former case, an abrupt drop of the surface pressure is visible in the isotherm when compressed beyond the collapse, but upon further compression either the stabilization or an increase of surface

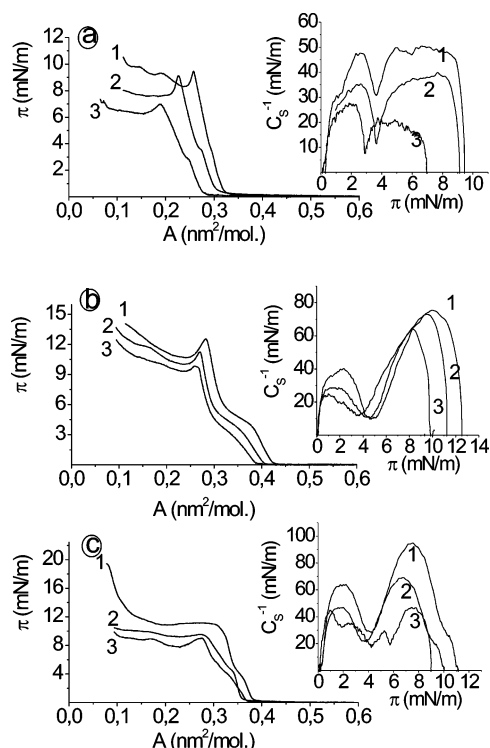


Figure 1. Surface pressure (π)–mean molecular area (A) isotherms and compression modulus (C_s^{-1})–surface pressure (π) dependencies (insets) registered for (a) F6H18, (b) F8H16, and (c) F10H14 at different subphase temperatures ($T(1) = 10\text{ }^{\circ}\text{C}$, $T(2) = 20\text{ }^{\circ}\text{C}$, and $T(3) = 30\text{ }^{\circ}\text{C}$).

pressure is usually observed. In the latter case, the surface pressure ceases to rise at the point of the isotherm corresponding to the collapse, and upon further compression π remains constant or slightly increases. The spike-like collapse occurs when the nucleation rate starts to be greater than the compression rate, leading to the decrease of surface pressure, whereas in the case of the plateau-like collapse, the nucleation rate equals the compression rate, and this leads to the stabilization of the pressure value. As observed in Figure 1, the collapse of F6H18 and F8H16 is spike-like at all the investigated temperatures, whereas in the case of F10H14 the collapse is plateau-like at 10 and 20 $^{\circ}\text{C}$; however, it is spike-like at a higher subphase temperature. Such a behavior seems to reflect different collapse mechanisms.

In the course of the π – A isotherm, a characteristic kink at about 4 mN/m appears, which is visible as a minimum in the course of the C_s^{-1} – π curves. Its existence was previously interpreted, on the basis of semiempirical calculations, as a transition from a dimeric double-helix to the monomeric organization of SFA molecules.³⁴ However, another interpretation of the kink is also possible. We tried here to estimate the equilibrium surface pressure of the investigated semifluorinated alkanes, which is not a trivial task. We obtained values of about 2.7–5.3 mN/m, which coincide with the isotherm region when the kink appears. Therefore, it is possible that the kink results from some nucleation process. If this was the case, the kink could simply correspond to the critical surface pressure, as defined by Gaines.¹ The monolayers of the three semifluorinated alkanes investigated here are homogeneous until the collapse pressure, as proved with BAM, and no nuclei are visible at the kink pressure or above it; however, their existence cannot be excluded, because their size can fall below BAM resolution. To have a deeper insight into this question, we measured the relaxation of monolayers below and slightly beneath the kink

pressure, that is, at 2 and 6 mN/m (5 mN/m for F6H18) (Figure 2). Generally, at 10 and 20 $^{\circ}\text{C}$ the monolayers are stable both at 2 and 6 (5) mN/m, and the decrease of the molecular area in time is negligible. The situation is slightly different at 30 $^{\circ}\text{C}$, since a fall of about 0.02 nm²/molecule is observed for all the investigated cases (Figure 2). It seems that the monolayer reorganization—and not the nucleation of the 3D phase—is responsible for the drop of molecular area observed here, as neither aggregates nor any 3D structures are visible in BAM images even after a long period of observation time.

Let us proceed now to the relaxation experiments at surface pressures close to π_c . In this kind of experiments, the monolayers were compressed to a surface pressure lower (of about 1 mN/m) than the collapse pressure, and afterward the compression mode was changed to quasi-static; the surface pressure was kept at a constant value and the evolution of molecular area in time was monitored. The resulting A – $\log t$ curves are gathered in Figure 3. The experiments were carried out continuously, but for a clear presentation, the point markers were included in the graph. Generally, all the curves have the form of sigmoidal decay. It is quite a typical form of the relaxation curve,¹⁵ since at the beginning of the experiment the nucleation begins and the nuclei grow freely in the monolayer, while their growth rate is limited mainly by the diffusion rate of the monolayer material into the 3D structures. However, after some period of time, the nuclei growth ceases to be free, because the collision process starts to be appreciable and finally the equilibrium between the monolayer material and the 3D structures is achieved, leading to a constant value of molecular area. The increase in temperature leads to a faster drop of the molecular area at the beginning of the experiment. A profound difference can be observed between the relaxation behavior of the first two compounds (F6H18 and F8H16) and F10H14, because in former cases it seems that regardless of the subphase temperature the decay of molecular area in time proceeds to a common asymptotic value, which is approximately three times smaller than the initial area, whereas such a trend is not observed for F10H14, in which case each of the A – $\log t$ curves has its own asymptote.

The evolution of the monolayer structure was monitored upon the relaxation experiments with Brewster angle microscope, and the representative images are shown in Figures 4–6.

Figure 4 presents selected images registered for F6H18 at the investigated subphase temperatures. Photos 4a–d illustrate the relaxation of the monolayer at 10 $^{\circ}\text{C}$. First aggregates appear about 200 s after the start of the relaxation experiment. They are quite large and polydisperse, as both circular and elongated domains can be simultaneously observed. The aggregation of the first domains proceeds rapidly, then they join together, forming larger islets (photo 4b), which collide with each other (photo 4c), and finally after approximately 1500 s the interface is covered by a multilayer, which is not ideally homogeneous as some black holes of the monolayer thickness can still be observed in it (photo 4d). At 20 $^{\circ}\text{C}$ the nucleation and growth of the 3D phase is similar but more rapid; however, the situation changes dramatically at 30 $^{\circ}\text{C}$. In about 100 s, ribbon-like structures can be observed (photo 4j), which grow anisotropically, forming dendritic domains, clearly visible in photo 4k. Further growth of the 3D phase does not lead to a homogeneous multilayer coverage. On the contrary, a complicated network of long, multiple interdigitated ribbon-like structures appears (photo 4l). Similar structures were also observed by other authors in the gel phase formed by SFAs.³⁵

The BAM images registered during the relaxation experiments for F8H16 monolayers are shown in Figure 5. At 10 $^{\circ}\text{C}$ first,

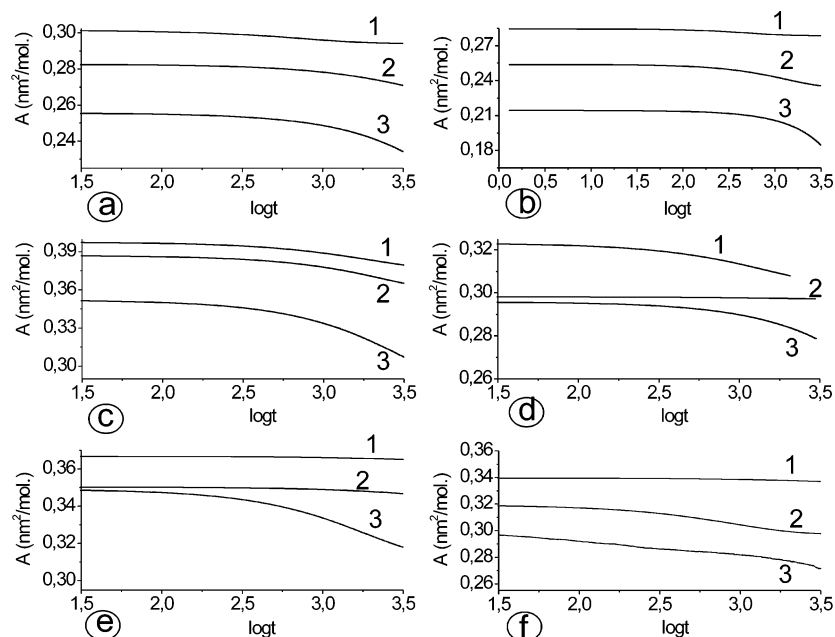


Figure 2. Mean molecular area (A)—logarithm time ($\log t$) dependencies registered at different subphase temperatures for: F6H18 at $\pi = 2 \text{ mN/m}$ (a) and at $\pi = 5 \text{ mN/m}$ (b); F8H16 at $\pi = 2 \text{ mN/m}$ (c) and at $\pi = 6 \text{ mN/m}$ (d); F10H14 at $\pi = 2 \text{ mN/m}$ (e) and at $\pi = 6 \text{ mN/m}$ (f). ($T(1) = 10^\circ\text{C}$, $T(2) = 20^\circ\text{C}$, and $T(3) = 30^\circ\text{C}$).

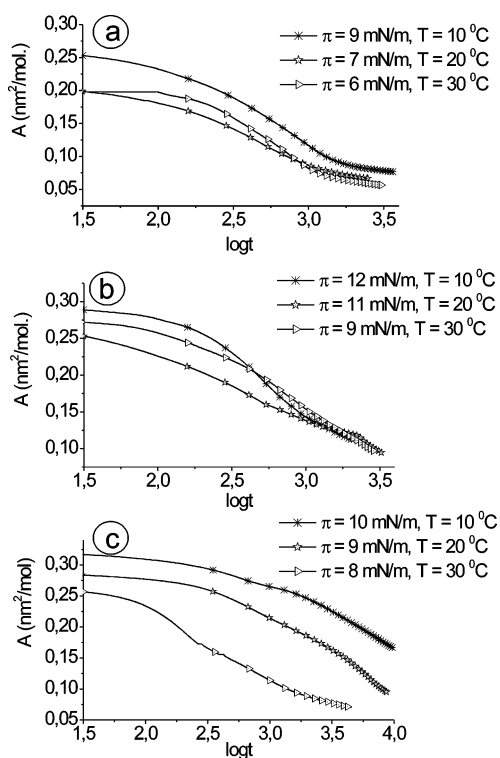


Figure 3. Mean molecular area (A)—logarithm time ($\log t$) curves registered for the investigated compounds at the monolayer collapse.

small circular nuclei, which are just at the limit of the microscope resolution, already can be seen after 60 s. The evolution of the monolayer toward the 3D structure is, however, pronouncedly different as compared to the above-described case of F6H18. What can be observed is the increase of the total number of nuclei with time, which are present in the view field of the microscope, but their size does not change and no fusion of the nuclei was observed. As the time increases (1000 s), the nuclei organize themselves forming parallel stripes at the surface (photo 5d), but it is clearly visible in this photo that they are separated. The presence of these stripes can be a manifestation

of some folding or fracturing process in the monolayer lying below. At 20 and 30°C the situation is different, because the observed structures are not monodisperse and their growth can be seen in BAM images. The homogeneous multilayer coverage is not achieved and the image after a long time at 20°C is similar to that taken at early stages of the F6H18 collapse. However, the diffuse edges of the domains, visible in photo 5h, are not artifacts and prove that the fusion of the nuclei into larger domains is not completed, and that the domains are composed of some smaller grains. At 30°C , the collapse of F8H16 begins to resemble that of F6H18 at the same temperature; however, the ribbon-like structures are not observed and the network forming domains seems to be composed of smaller grains.

The results of the BAM observations of the F10H14 collapse are gathered in Figure 6. The images observed at 10°C are very similar to those recorded at the same temperature for F8H16. The difference between these two compounds lies in the nucleation and growth rates. The evolution of the F10H14 collapse at 10°C is extremely slow as compared to the SFAs with a shorter perfluorinated moiety. The observed monolayer is homogeneous, and not earlier than after 1000 s first nuclei start to appear. The first nuclei are scattered at the interface and their number is low. The BAM image observed here after 4000 s is similar to that for F8H16 after 10 times shorter time. The further steps of the F10H14 collapse at 10°C also resemble the collapse of F8H16 as far as the increase in the number of the nuclei is concerned, but their size remains unchanged. After 9000 s, some clustering of the nuclei along parallel lines can also be observed (photo 6d). At 20°C the evolution of the F10H14 collapse is also similar to that discussed for F8H16, as also here polydispersity of the 3D domains' sizes occurs. The rate of the 3D phase growth is also slow at this temperature. In contrast, the increase of temperature to 30°C leads to a dramatic increase of the growth rate, that is, first nuclei are already visible after 200 s (photo 6i) and their growth is fast, in a manner similar to that observed for F8H16 at this temperature. The difference is that even after a long period of time the network of anisotropically elongated domains was not observed.

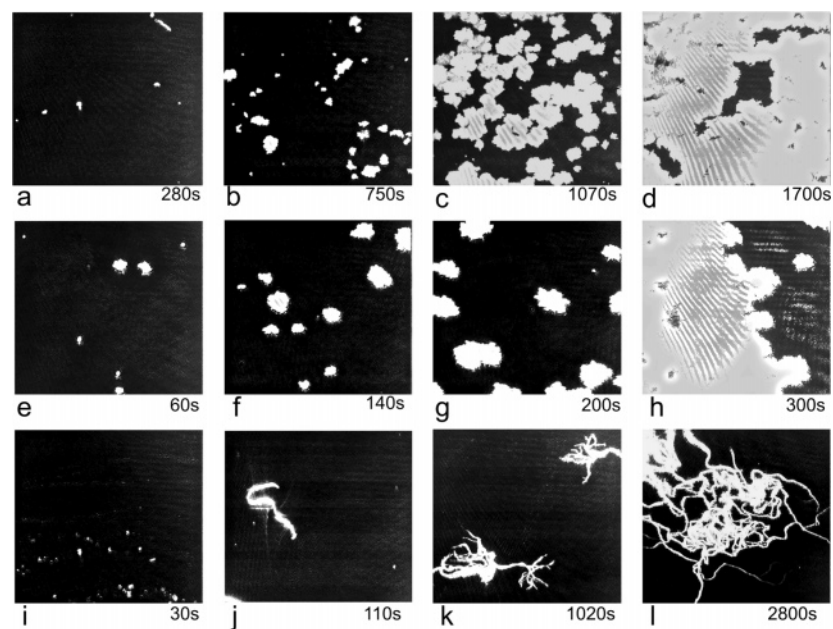


Figure 4. BAM images of the evolution of the 3D phase formation from F6H18 monolayer at its collapse. (a–d) $T = 10\text{ }^{\circ}\text{C}$, (e–h) $T = 20\text{ }^{\circ}\text{C}$, and (i–l) $T = 30\text{ }^{\circ}\text{C}$.

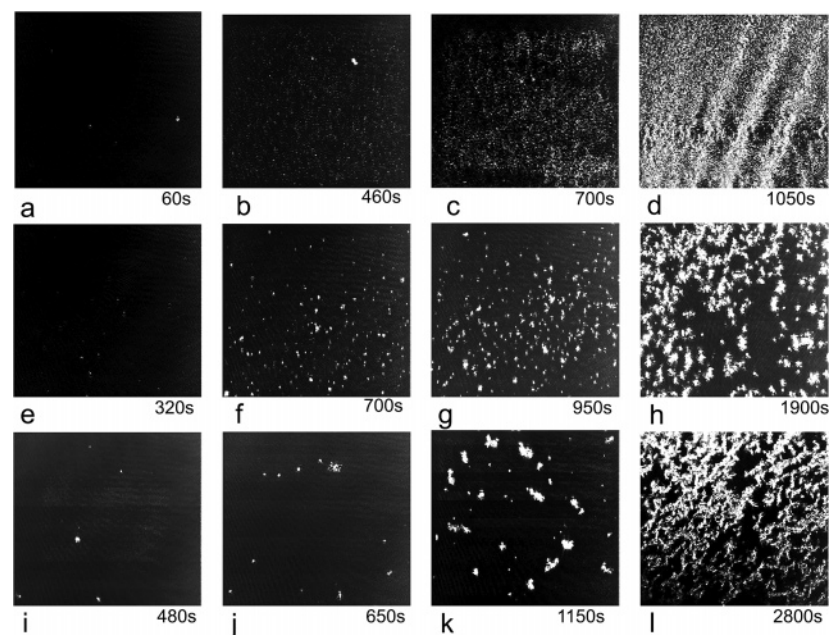


Figure 5. BAM images of the evolution of the 3D phase formation from F8H16 monolayer at its collapse. (a–d) $T = 10\text{ }^{\circ}\text{C}$, (e–h) $T = 20\text{ }^{\circ}\text{C}$, (i–l) $T = 30\text{ }^{\circ}\text{C}$.

Discussion

To have a deeper insight into the collapse process of the investigated monolayers, the nucleation–growth–collision theory was applied.^{15–17} In this approach, the authors derived the following relation regarding the relaxation of the molecular area in time at the monolayer collapse:

$$\frac{A_0 - A}{A_0 - A_{\text{inf}}} = 1 - \exp(-K_x(t - t_i)^x) \quad (1)$$

where A is the molecular area at any time, A_0 is the initial molecular area, and A_{inf} is the molecular area in the limit of infinite time. K_x and t_i (called the induction time) are constants, the origin of which is described in detail in the source paper.¹⁵ Here, a very important parameter is the exponent x , the value

of which depends on the geometrical conditions concerning the shape and means of growth of the 3D nuclei as well as on the kinetics of the growth. Generally, the authors focus their attention on two starting geometries of the nuclei—hemispherical and cylindrical, and define two ways of the growth process—the edge growth (when the new material from the monolayer is incorporated into the 3D nucleus at its edges) and the basal growth, at which the nuclei grow from their basal area. As far as the kinetics of the process is concerned, two limiting cases are distinguished: the growth can be instantaneous (leading to monodispersed nuclei) or progressive (leading to polydispersity of their sizes). Therefore, for the edge growth of hemispherical nuclei, $x = 1.5$ or 2.5 (instantaneous or progressive growth, respectively), whereas in the case of a cylindrical edge growth, $x = 2$ or 3 (instantaneous or progressive). For the basal growth,

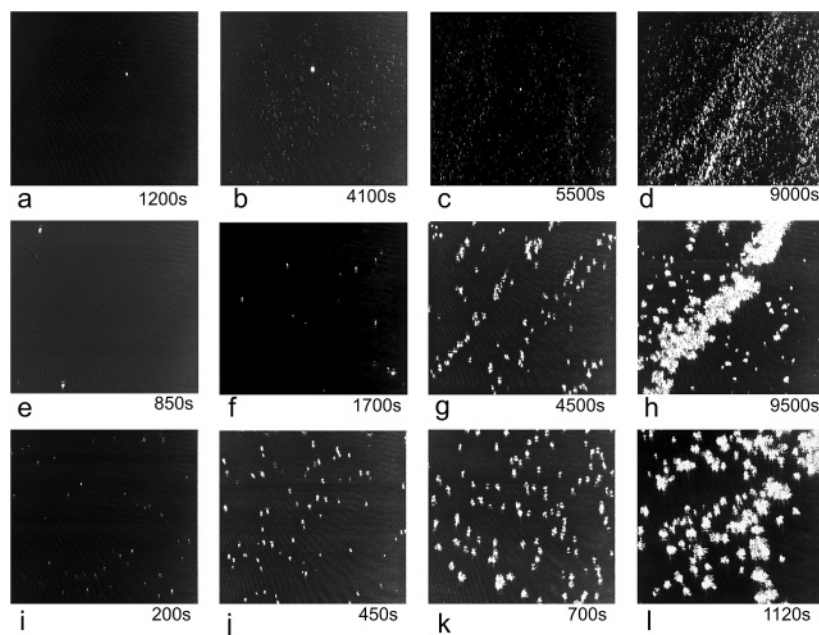


Figure 6. BAM images of the evolution of the 3D phase formation from F10H14 monolayer at its collapse. (a–d) $T = 10\text{ }^{\circ}\text{C}$, (e–h) $T = 20\text{ }^{\circ}\text{C}$, (i–l) $T = 30\text{ }^{\circ}\text{C}$.

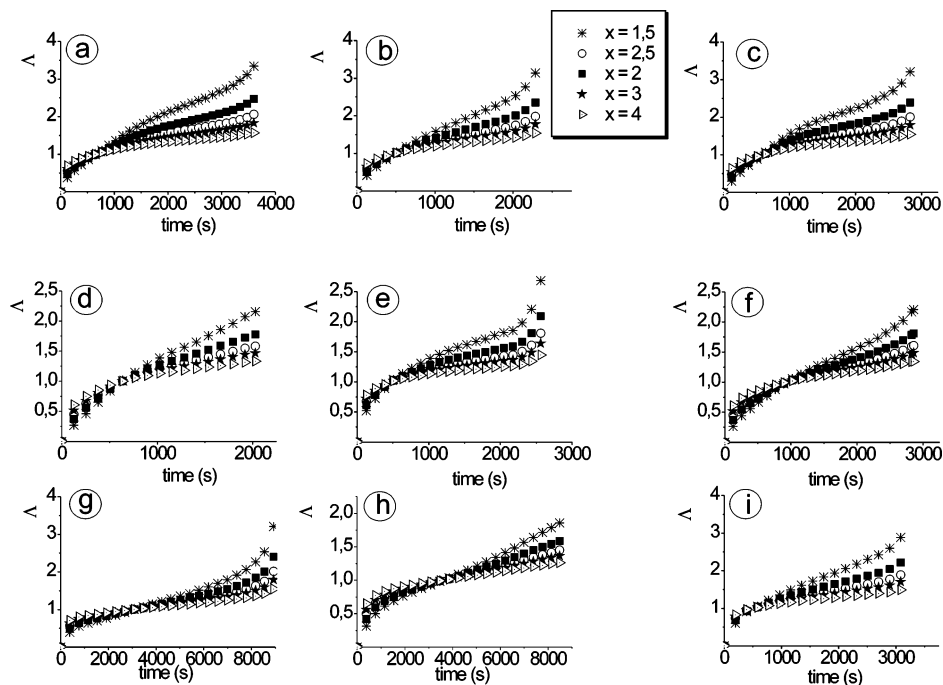


Figure 7. The Λ -time curves illustrating the search for the best value of the exponent x from the nucleation-growth-collision theory model. (a–c) F6H18, (d–f) F8H16, (g–i) F10H14. (a, d, g) $T = 10\text{ }^{\circ}\text{C}$; (b, e, h) $T = 20\text{ }^{\circ}\text{C}$; (c, f, i) $T = 30\text{ }^{\circ}\text{C}$.

$x = 3$ or 4 (instantaneous or progressive). The logarithm of eq 1 has the following form:

$$\left(\ln \left(\frac{1}{1 - (A_0 - A)/(A_0 - A_{\text{inf}})} \right) \right)^{1/x} = -K_x^{1/x} (t - t_i) \quad (2)$$

As can be easily noticed, this is an equation of the linear dependence of the left-hand-side argument of time. The procedure of the relaxation data interpretation according to this model is as follows. The left-hand-side expression is calculated for the experimental data with all the exponents, and then the five sets of data are plotted vs time. If the exponent x is fitted correctly, the plot should be linear. Generally, the linear

regression procedure is applied, and the curve of the best fit (the highest correlation parameter R and the lowest standard deviation) proves the correctness of one of the possible growth mechanisms.^{15,16} This procedure was applied herein to interpret the relaxation curves in Figure 3. The resultant plots are shown in Figure 7. To avoid the repetition of the left-hand-side expression of eq 2 in each plot, it was denoted as Λ . The value of A_{inf} was estimated in each case by fitting sigmoidal decay curves to the experimental A -log t dependencies. Values of A_0 and A_{inf} are gathered in Table 1.

As can be noticed, in all the plots in Figure 7, parts a–i, the best fitted are the curves obtained for the exponent $x = 3/2$, which was proved by the linear regression; however, the curves

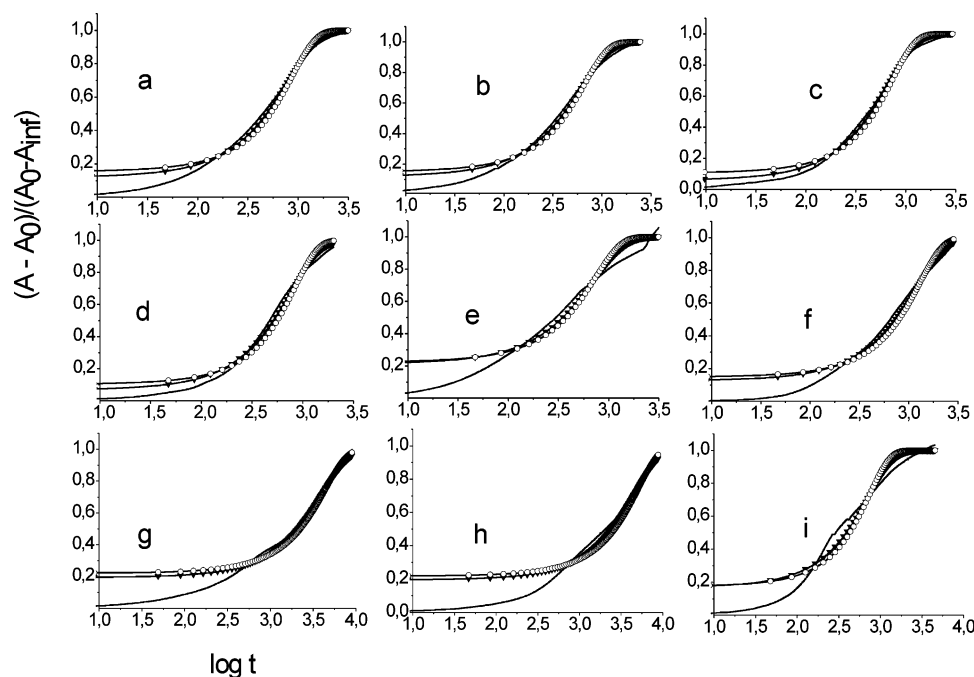


Figure 8. Fitting of the experimental data $(A_0 - A)/(A_0 - A_{\text{inf}})$ (solid curve) by the plots calculated from the Vollhardt model for the instantaneous hemispherical growth of the nuclei (solid curve marked with filled triangles) and progressive hemispherical growth of the nuclei (solid curve marked with open circles).

TABLE 1: Initial Molecular Areas (A_0) and the Molecular Areas Estimated at the Infinite Time (A_{inf}) Applied for the Calculations of the Expression A in the Nucleation–Growth–Collision Theory Model

compound	10 °C		20 °C		30 °C	
	A_0 (nm ² /mol)	A_{inf} (nm ² /mol)	A_0 (nm ² /mol)	A_{inf} (nm ² /mol)	A_0 (nm ² /mol)	A_{inf} (nm ² /mol)
F6H18	0.263	0.077	0.209	0.066	0.198	0.055
F8H16	0.295	0.105	0.270	0.105	0.275	0.090
F10H14	0.372	0.152	0.288	0.080	0.265	0.0765

for $x = 5/2$ (progressive spherical growth) does not also deviate significantly from linearity. The linearization of the curves obtained from the Vollhardt model enables the estimation of the kinetic constant K_x and the induction time t_i . Knowing these parameters it is possible to fit the experimental data with the curves calculated from the applied model. It was done for the hemispherical instantaneous and progressive growth and shown in Figure 8. The conclusions are that the experimental points expressed as $(A_0 - A)/(A_0 - A_{\text{inf}})$ are well fitted with both curves calculated for instantaneous (solid curve) and progressive (dotted curve) growth of the nuclei. The theoretical curves fail to fit the experimental data at the very beginning of the experiment, later the calculated curves virtually overlap with the experimental curve, and at very large observation times some distortions of the theoretical curves from the experimental results are visible. Both curves calculated for the exponent $3/2$ and $5/2$ (instantaneous and progressive hemispherical growth of the 3D nuclei, respectively) are well fitted to the experimental points; however, it can be observed that the curve for the exponent $3/2$ reproduces the experimental results slightly better than in the case of the exponent $5/2$. However, it should be stated here that the division of the nucleation models discussed here into instantaneous and progressive is slightly artificial. In the nucleation–growth–collision theory, Vollhardt and Retter¹⁵ apply the foundations of the Avrami theory of crystal growth,³⁶ according to which the kinetics of nucleation is given by the following equation:

$$N = N_{\text{max}}(1 - \exp(-k_n t)) \quad (3)$$

where N is the number of nuclei at any time, N_{max} is the total number of nuclei, and k_n is the nucleation rate constant. For large k_n values the nucleation is defined to be instantaneous, whereas for small k_n values the nucleation is called progressive. However, apart from these two limiting cases, there is a whole spectrum of intermediate k_n values for which it is difficult to discriminate conclusively over the instantaneous and progressive nucleation model, which can be the case of the semifluorinated alkanes discussed here.

The instantaneous hemispherical growth is more probable for F8H16 and F10H14 than for F6H18, as it leads to monodisperse 3D structures. This can be proved with BAM photos registered for the collapsed phases of F8H16 and F10H14 at 10 °C. Only small circular domains of uniform size can be observed in Figures 5 and 6 (photos a–d). For the collapsed monolayers of F8H16 and F10H14 at 20 and 30 °C, the hemispherical instantaneous growth mechanism seems also to be legitimized, as even if the polydispersity of the domains is observed, the domains appear to be composed of smaller grains of the uniform size. The nucleation–growth–collision model seems to fail to describe the collapse of the monolayers of F6H18; however, this can be an oversimplification. As it was underlined upon describing the BAM images of the collapsing F6H18 films, the whole collapse process of the monolayers of this compound is much faster than for the SFAs with longer perfluorinated moiety. The theory describes three phenomena, which are specified in its name. It is probable that in the case of F6H18 the step of nucleation has kinetics similar to that of the two other SFAs investigated here, but differences start at the level of growth,

and especially coalescence of the growing 3D domains. The shortest perfluorinated moiety and the longest hydrogenated chain as compared to F8H16 and F10H14 can lead to the increase of the van der Waals forces between the F6H18 molecules, being the reason for the increased rate of the growth of the collapsed structures and their propensity to coalescence.

A very interesting feature of the Λ - t curves shown in Figure 7 is the particular t value at which the curves calculated for all the five possible values of the exponent x value intersect. This can be interpreted as a time at which the rate of collision and/or fusion of the 3D structures equals the rate of their growth. It is visible in the Λ - t plots that it is about 600 s for F6H18 and F8H16 regardless of the subphase temperature. For F10H14, this value is 5 times as large, that is, about 3000 s at 10 and 20 °C; however, it drops dramatically at 30 °C, reaching the value of about 600 s, typical for the SFAs with shorter perfluorinated segments. The profound differences in the 3D phase formation kinetics between F10H14 at lower temperatures and F8H16 and F6H18 can explain different collapse types observed in Figure 1. F6H18, F8H16 (and F10H14 at 30 °C) show a spike-like collapse, while F10H14 at lower subphase temperatures shows a collapse of the plateau-like type. In the case of spike-like collapse, the 3D phase formation rate is greater than the compression rate of the monolayer, leading to the fall of the surface pressure after π_c , whereas later on, both rates equilibrate and the surface pressure remains constant, or if the compression speed overgrows the rate of 3D phase formation, π begins to rise as shown in Figure 1b. In the case of F10H14, the rate of compression equals the 3D phase formation rate at π_c , and a long plateau region of the constant surface pressure value can be observed in the π - A isotherm. At a low molecular area value, when the collision process slows down the 3D phase formation, the compression rate again begins to dominate and a steep increase of the π -value can be observed in the isotherm. An interesting question arises also regarding the number of the layers present in the 3D structures formed in the collapsed films. The drop in the molecular area observed for F6H18 and F8H16 from the initial A_0 value to the limiting A_{inf} , which is approximately three times smaller (see Table 1), can lead to the conclusion that trilayer structures are formed; however, this should be proved by further experiments.

Conclusions

Our results prove that the nucleation-growth-collision theory not only can be applied to the monolayers of typical surfactants, such as long-chain carboxylic acids, but also can be successfully employed for the modeling of the collapse process in monolayers of primitive, partially fluorinated surfactants, like semifluorinated alkanes. There was quite a good agreement between the BAM observations and the conclusion drawn, that the growth of the 3D phase is instantaneous and the 3D nuclei are hemispherical. The model fails partially to interpret the collapse of the compound containing the shortest fluorinated part: F6H18; however, it seems to originate from a specific fusion of the 3D nuclei into long ribbon-like structures, the form of which is similar to the organization of some SFAs in their gel phases in organic liquids. The different collapse

types of the monolayers of F8H16 and F6H18 (spike-like) and F10H14 (plateau-like) were ascribed to the differences in the nucleation and growth observed for the investigated chemicals.

Acknowledgment. This work was supported by Ministerio de Ciencia y Tecnología (Grant CTQ2006-04085) and Xunta de Galicia (Grant PGIDT06PXIB383004PR).

References and Notes

- (1) Gaines, G. L., Jr. *Insoluble Monolayers at Liquid-Gas Interfaces*; John Wiley & Sons: New York, 1966.
- (2) Bibb, A. M.; Knobler, C. M.; Petersen, I. R. *J. Phys. Chem.* **1991**, *95*, 5591–5594.
- (3) Kaganer, V. M.; Loginov, E. B. *Phys. Rev. E* **1995**, *51*, 2237–2249.
- (4) Angelova, A.; Vollhardt, D.; Ionov, R. *J. Phys. Chem.* **1996**, *100*, 10710–10720.
- (5) Alig, T. F.; Warriner, H. E.; Lee, L.; Zasadzinski, J. A. *Biophys. J.* **2004**, *86*, 897–904.
- (6) Gopal, A.; Lee, K. Y. C. *J. Phys. Chem. B* **2006**, *110*, 22079–22087.
- (7) Yan, W.; Piknova, B.; Hall, S. B. *Biophys. J.* **2005**, *89*, 306–314.
- (8) Zhang, Y.; Fischer, T. M. *J. Phys. Chem. B* **2005**, *109*, 3442–3445.
- (9) Birdi, K. S.; Vu, D. T. *Langmuir* **1994**, *10*, 623–625.
- (10) Hattar, E.; Fischer, T. M. *J. Phys. Chem. B* **2002**, *106*, 589–592.
- (11) Kundu, S.; Datta, A.; Hazra, S. *Langmuir* **2005**, *21*, 5894–5900.
- (12) Nikomarov, E. S. *Langmuir* **1990**, *6*, 410–414.
- (13) Ries, H. E., Jr. *Nature* **1979**, *281*, 287–289.
- (14) Smith, R. D.; Berg, J. C. *J. Colloid Interface Sci.* **1980**, *74*, 273–286.
- (15) Vollhardt, D.; Retter, U. *J. Phys. Chem.* **1991**, *95*, 3723–3727.
- (16) Vollhardt, D.; Retter, U.; Siegel, S. *Thin Solid Films* **1991**, *199*, 189–199.
- (17) Vollhardt, D.; Retter, U. *Langmuir* **1992**, *8*, 309–312.
- (18) Retter, U.; Vollhardt, D. *Langmuir* **1993**, *9*, 2478–2480.
- (19) Vollhardt, D.; Ziller, M.; Retter, U. *Langmuir* **1993**, *9*, 3208–3211.
- (20) Avila, L. V. N.; Saraiva, S. M.; Oliveira, F. M. *Colloids Surf., A: Physicochem. Eng. Aspects* **1999**, *154*, 209–217.
- (21) Lo Nostro, P.; Chen, S. H. *J. Phys. Chem.* **1993**, *97*, 6535–6540.
- (22) Binks, B. P.; Fletcher, P. D. I.; Sager, W. F. C.; Thompson, R. L. *Langmuir* **1995**, *11*, 977–983.
- (23) Gaines, G. L., Jr. *Langmuir* **1991**, *7*, 3054–3056.
- (24) Mourran, A.; Tartsch, B.; Gallyamov, M.; Magonov, S.; Lambreva, D.; Ostrovskii, B. I.; Dolbnya, I. P.; de Jeu, W. H.; Moeller, M. *Langmuir* **2005**, *21*, 2308–2316.
- (25) Huang, Z.; Acero, A. A.; Lei, N.; Rice, S. A.; Zhang, Z.; Schlossman, M. L. *J. Chem. Soc., Faraday Trans.* **1996**, *92*, 545–552.
- (26) El Abed, A.; Pouzet, E.; Faure, M. C.; Saniere, M.; Abillon, O. *Phys. Rev. E* **2000**, *62*, R5895.
- (27) Wang, S.; Lunn, R.; Krafft, M. P.; Leblanc, R. M. *Langmuir* **2000**, *16*, 2882–2886.
- (28) Krafft, M. P.; Giulieri, F.; Fontaine, P.; Goldmann, M. *Langmuir* **2001**, *17*, 6577–6584.
- (29) Broniatowski, M.; Miñones, J., Jr.; Sandez Macho, I.; Dynarowicz-Łątka, P. *Pol. J. Chem.* **2005**, *79*, 1047–1061.
- (30) Broniatowski, M.; Nieto Suarez, M.; Vila Romeu, N.; Dynarowicz-Łątka, P. *J. Phys. Chem. B* **2006**, *110*, 19450–19455.
- (31) Rabolt, J. F.; Russell, T. P.; Twieg, R. J. *Macromolecules* **1984**, *17*, 2780–2794.
- (32) Broniatowski, M.; Sandez Macho, I.; Miñones, J., Jr.; Dynarowicz-Łątka, P. *J. Phys. Chem. B* **2004**, *108*, 13403–13411.
- (33) Davies, J. T.; Rideal, E. K. *Interfacial Phenomena*; Academic Press: New York, 1963.
- (34) Dynarowicz-Łątka, P.; Perez Morales, M.; Muñoz, E.; Broniatowski, M.; Martin Romero, M. T.; Camacho, L. *J. Phys. Chem. B* **2006**, *110*, 6095–6100.
- (35) Lo Nostro, P.; Ku, C. Y.; Chen, S. H.; Lin, J. S. *J. Phys. Chem.* **1995**, *99*, 10858–10864.
- (36) Avrami, M. *J. Chem. Phys.* **1939**, *7*, 1103–1112.